PAPER

Observation of the high-density front at the high-field-side in the J-TEXT tokamak

To cite this article: Peng Shi *et al* 2021 *Plasma Phys. Control. Fusion* **63** 125010

View the article online for updates and enhancements.

Observation of the high-density front at the high-field-side in the J-TEXT tokamak

Peng Shi[1,2,3] ⓘ**, Hongjuan Sun**[1] ⓘ**, Ge Zhuang**[4,]***, Zhifeng Cheng**[3] ⓘ**, Li Gao**[3]**,
Zhipeng Chen**[3] ⓘ**, Jingchun Li**[5] ⓘ**, Yinan Zhou**[3]**, Chengxi Zhou**[3] **and the J-TEXT Team**

[1] United Kingdom Atomic Energy Authority, Culham Centre for Fusion Energy, Culham Science Centre, Abingdon, Oxon OX14 3DB, United Kingdom
[2] Southwestern Institute of Physics, PO Box 432, Chengdu 610041, People's Republic of China
[3] International Joint Research Laboratory of Magnetic Confinement Fusion and Plasma Physics, State Key Laboratory of Advanced Electromagnetic Engineering and Technology, School of Electrical and Electronic Engineering, Huazhong University of Science and Technology, Wuhan 430074, People's Republic of China
[4] School of Physical Sciences, University of Science and Technology of China, Hefei, Anhui 230026, People's Republic of China
[5] Department of Earth and Space Sciences, Southern University of Science and Technology, 518055 Shenzhen, Guangdong, People's Republic of China

E-mail: gezhuang@ustc.edu.cn and peng.shi@ukaea.uk

Abstract

This article reports the observation of the high-density front at the high field side (HFS) region in the limiter J-TEXT tokamak. In the J-TEXT high density discharges, the high-density front at the HFS scrape-off layer (SOL) region has been clearly identified by the far-infrared laser polarimeter-interferometer. The high-density front forms at the HFS SOL when the plasma density reaches a critical value, it can be up to seven times higher than the density in the low field side region and it stays stable as long as the density remains. In this stable phase, the local radiation is at a low level and it shares common characteristics with the high-field-side high-density (HFSHD) phenomena observed in divertor devices. If density increases continuously, the high-density front expands poloidally and evolves into an unstable 'moving' phase while propagating into the main plasma region, which eventually triggers the disruption. The maximum achievable density on J-TEXT seems to be correlated with the evolution of the high-density front, suggesting that the region may play a role in setting the operational limit on J-TEXT. The unstable phase of high-density front seems to share some common characteristics with the well-known multifaceted asymmetric radiation from the edge (MARFE), except that the radiation level in J-TEXT stays at a low level. The density threshold of the high-density front formation and the maximum density of the region itself increase with I_P, consistent with the observation on both HFSHD and MARFE. The MARFE-like behavior of the high-density front in its final stage, suggests that MARFEs might be the result of these fronts forming in or moving into regions where the plasma temperature and impurity concentration are conducive for them to be radiatively unstable.

---

* Author to whom any correspondence should be addressed.

1. Introduction

High density operation can lead to a high thermonuclear power gain, and also be preferential for achieving steady heat flux that is compatible with the material limits of the first wall and divertor target [1]. Therefore, high density operation is highly desirable for the next-step tokamaks, such as the International Thermonuclear Experimental Reactor [2] and Chinese Fusion Engineering Testing Reactor [3]. Nevertheless, the occurrence of density limit (DL) disruption is a great obstacle for high density operation [4]. As plasma density approaches a limit, radiative-thermal instabilities induced by radiations from light impurities like carbon and oxygen, such as MARFE (multifaceted asymmetric radiation from the edge) and radiative divertor, are often observed [5–7]. Although the highly radiative edge helps to reduce the heat flux to limiter/divertor, it is often associated with a substantial degradation of global energy confinement and sometimes with DL disruptions. Thus, it is important to study the properties of edge plasma in high density tokamak operation.

MARFEs, the first radiative-thermal instability discovered in tokamaks, have been widely observed on various limiter and divertor devices [8–11]. MARFEs are believed to be the result of an instability which arises when a local change in the radiated power, brought about by a temperature perturbation, is higher than the compensatory heat flow. Thus, MARFEs usually form in the region where the thermal flow is reducing, i.e. in the limiter plasmas they mostly locate at the high field side (HFS) near the inner wall [12, 13], while in the divertor plasmas, they tend to be located close to the X-point region [7, 14]. The term 'MARFE' is commonly used to refer only to MARFEs in limiter plasmas, and MARFEs in divertor plasmas, which is usually accompanied with divertor detachment, is named as 'X-point MARFE' or 'divertor MARFE'.

In recent years, a so-called high-field side high-density (HFSHD) phenomenon, which is related to divertor detachment and X-point MARFE, has been observed in divertor high-density plasmas on Asdex-Upgrade (AUG) and Joint European Torus (JET) [15–18]. In these studies, when the inner divertor is detached while the outer divertor stays attached, a poloidally localized high-density region occurs in the HFS scrape-off layer (SOL) which extends from X-point towards the HFS mid-plane [18]. This region is known as the HFSHD front. Simulations by scrape off layer plasma simulator (SOLPS) show that the HFSHD front plays an important role in the fuelling of the core plasma and thus can lead to strong change in global performance [17]. At first, the HFSHD front forms near the inner target. When plasma density further increases, the HFSHD front moves towards the X-point and then complete detachment and a X-point MARFE occurs [15]. The HFSHD shares some features with MARFE, such as localized high-density and low-Z impurity emission, and

a threshold density correlated with plasma current. However, MARFEs are characterized by a radiative unstable region, whereas the HFSHD has a stable region with relatively low radiation power. In divertor plasma, the HFSHD front seems like the early-stage of X-point MARFE.

Recently, the high-density front has been observed at the HFS SOL region in J-TEXT tokamak, which shares some common features with both MARFE and HFSHD. The paper reports the characteristics of the high-density front on J-TEXT and compares with those in MARFE and HFSHD. The rest of the paper is organized as follows: section 2 describes the experimental setup and main diagnostics for the investigation of the HFSHD front in the J-TEXT tokamak; section 3 presents the observations which clearly show the formation and development of the HFSHD front in density ramping discharges; section 4 gives the influences of the global plasma current and edge plasma parameters on the properties of HFSHD front; section 5 provide the discussion and summary.

2. Experimental setup

The J-TEXT tokamak (formerly TEXT-U [19]) is a conventional medium-sized tokamak with a major radius of $R_0 = 1.05$ m and minor radius of $a = 0.25 - 0.29$ m (set by the silicon-carbide coated graphite limiter). The first wall and the limiter are covered with carbon tiles. Therefore, the dominating impurity in the J-TEXT is carbon. The discharges are performed with Ohmic heating and the working gas is hydrogen. Continuous gas-puffing is used to raise the plasma density in a single shot. In the experiments, the plasma parameters are $I_P = 120 - 170$ kA, $B_T = 1.7 - 2.1T, q_a = 4 - 5.5, a = 0.255$ m. The maximum density in J-TEXT Ohmic plasma is well below the Greenwald density, near $0.7n_G$, where n_G is the Greenwald density equal to $I_P / (\pi a^2)$ with I_p in units of MA and a in units of meter. Figure 1 depicts the main diagnostics used to record the formation and evolution of the HFSHD front in J-TEXT. The line-integrated electron density is measured by a 17-channel far-infrared laser polarimeter-interferometer system (POLARIS) [20], which views the plasma vertically at intervals of 3 cm on the radial mid-plane from $r = -24$ cm to $r = +24$ cm and covers the plasma poloidal cross-region from $-0.94a$ to $0.94a$, where $r = R - R_0$. Here, $r < 0$ and $r > 0$ corresponds to HFS and low-field-side (LFS), respectively. A 26-channel photodiode array (PDA) system is used to measure the line emission of carbon III (C_{III}) at the wavelength of 465 nm. As similar to POLARIS, the C_{III} array also covers both the HFS and LFS of the tokamak. The inner-most three chords—emphasized in figure 1—view the region where the HFSHD front is located. In addition, J-TEXT has a 32-channel bolometer array which detects the total radiation losses and covers the entire plasma cross section with spatial resolution of 21 mm [21], as well as a charge coupled device (CCD) camera
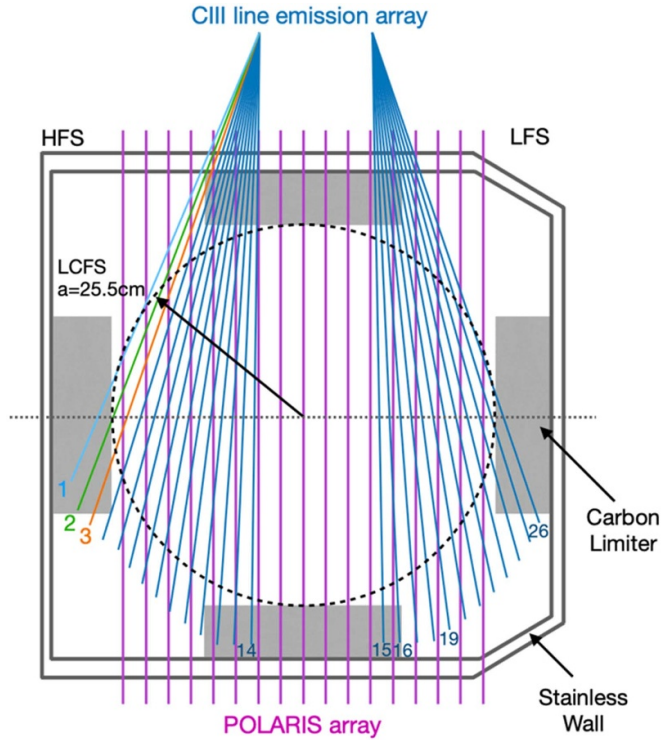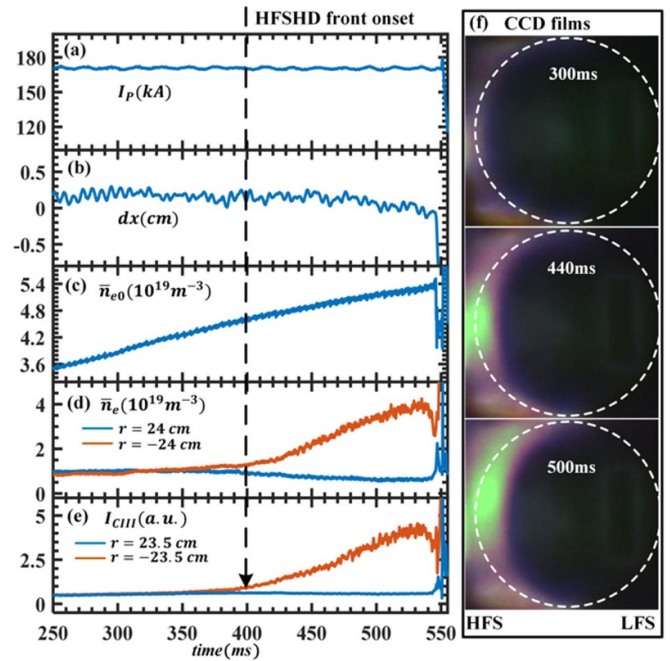
Figure 1. Viewing lines of the J-TEXT PDA (in blue color) and POLARIS (in magenta color), respectively.

Figure 2. Time evolution of the main parameters for a typical discharge (#39669) of density ramping to limit disruption in J-TEXT, indicating that the high-density front occurs at 400 ms. (a) Total plasma current, (b) horizontal plasma displacement, (c) central line-average electron density, (d) line-average electron density at the most HFS and LFS edge measured by POLARIS, (e) line emission of C_{III} measured by PDA, (f) visible CCD camera films, where the dotted circles denote the LCFS.

system which measures the visible emission distribution with a temporal resolution of 5 ms.

## 3. Experimental observation of the high-density front at HFS edge region

The temporal traces for a typical density-ramp discharge with a high-density front is shown in figure 2. The discharge has $I_P = 170$ kA, $B_T = 2.1T, q_a = 3.9$. The speed of gas-puff fueling was constant during the current flat-top. A DL disruption occurs at $t = 545$ ms and the maximum central line-average density is $\bar{n}_{e0} = 5.4 \times 10^{19}$ m$^{-3} = 0.65 n_G$. During the interval of 250 ms $< t <$ 540 ms, the central (at $r = 0$ cm) line-average electron density increases steadily (figure 2(c)). The line-average density at $r = -24$ cm (very edge of HFS) also increases throughout this period, but there is a rise in its rate of increase from about $t = 400$ ms. The line-average density at the very edge on the LFS ($r = 24$ cm) changes little throughout the same period, as shown in (figure 2(d)). Concomitantly, the C_{III} emission at the HFS edge also increases, as indicated in figure 2(e). This shows that a local high-density plasma region has formed in the HFS edge as the plasma density exceeds a critical value ($n_{crit} = 4.6 \times 10^{19}$ m^{-3} in this discharge). Such observations characterize the typical features of the HFSHD front phenomenon, as described in [16, 17]. In addition, the location and evolution of the high-density front were recorded by the visible CCD camera, as shown in figure 2(f). The dotted circle in figure 2(f) denotes the last closed flux surface (LCFS), determined by the position of the limiter. Before the onset of the high-density front ($t = 300$ ms), the visible line

radiation at the plasma boundary is very weak and approximately symmetric. However, after the formation of the high-density front ($t = 440$ ms), a bright spot appears on the HFS of the mid-plane, located mainly outside the LCFS. Moreover, by comparing the CCD films at 440 and 500 ms, it is seen that the bright spot expands poloidally and moves into the main plasma as the density further increases. Clearly, the location of the bright spot on the visible CCD film corresponds to the region of the high-density front. Thus, the CCD picture is a favorable instrument to study the evolution and movement of the high-density front.

Figure 3 shows profiles of the line-average electron density (figure 3(a)), line-integral C_{III} emission intensity (figure 3(b)) and total radiation power (figure 3(c)) during the HFSHD front formation, measured with the diagnostics and lines of sight shown in figure 1. During the interval of 400 ms $< t <$ 530 ms, the electron density at the HFS edge increases significantly, while that in the other channels varies little. This indicates that the HFSHD front is highly localized in the inner, HFS region, and the bulk of the confined plasma ($r > -20$ cm) remains almost unchanged. At the final stage of the discharge, the line-average density across the high-density front ($r = -24$ cm) reaches 4×10^{19}m^{-3}, which is seven times higher than that of the LFS region and almost comparable to the central density. The C_{III} emission shows a similar behavior with electron density, i.e. locally increases at the HFS edge. Upon the total radiation power, the asymmetry between the HFS and LFS edge
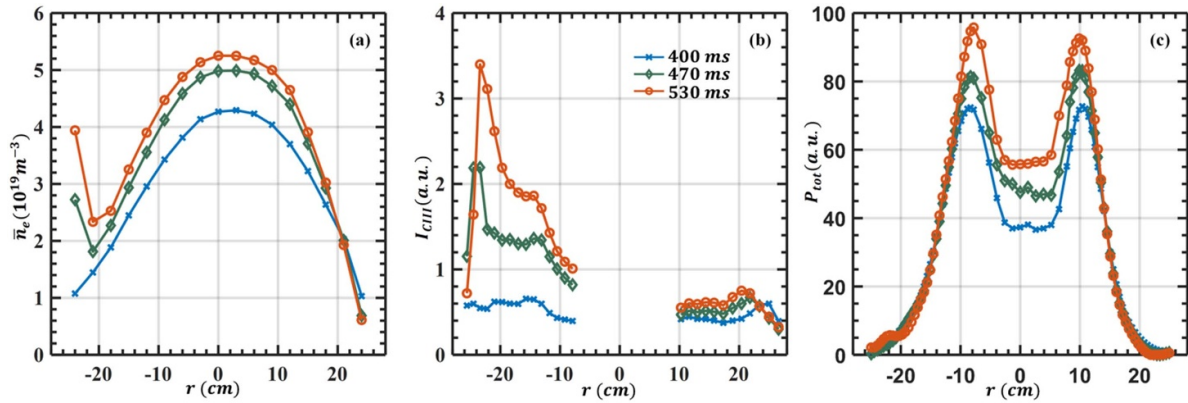
Figure 3. Corresponding to figure 2, time evolution of the radial distributions of (a) line-average electron density measured by POLARIS, (b) line-integral C_{III} radiation intensity obtained by the PDA array, and (c) radiation power detected by bolometer.
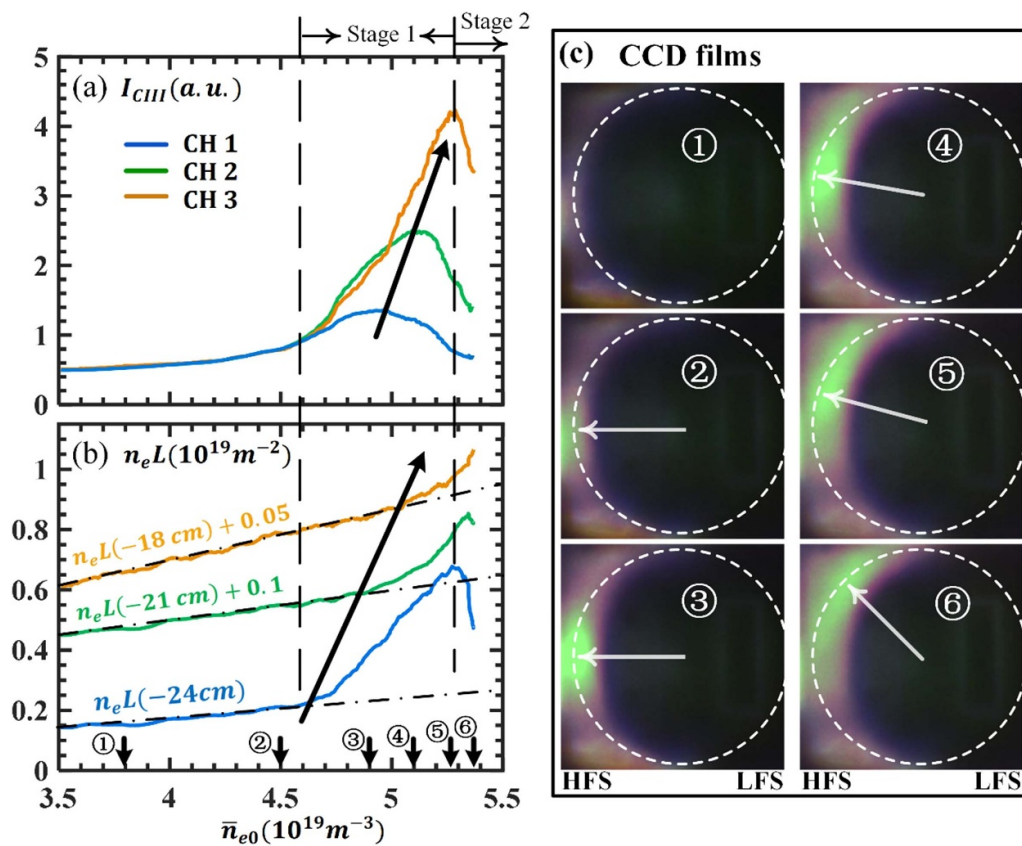
Figure 4. Corresponding to figure 2, traces of the three inner-most chords of (a) C_{III} emission and (b) line-integral electron density with the central line-average electron density. (c) Visible CCD camera films at six-time pieces corresponding to the black arrows on the *X*-axis of figure 2(b). The dotted circles denote the LCFS.

can also be seen, but comparing with the center region, the radiation at HFS edge is extremely small. And the ratio of total radiation to Ohmic heating power is less than 30%. It means that the high-density front observed on J-TEXT is different to the common MARFE phenomenon which is mainly featured as high radiation losses at edge [5].

More details of the evolution of the high-density front with continuous increase of the density, is illustrated in figure 4. The three inner-most channels of the C_{III} emission and electron density are plotted in figures 4(a) and (b) respectively.

Figure 4(c) shows six visible CCD pictures, which corresponds to the six points in figure 4(b), indicated by arrows on the *X*-axis. Low emission is observed at the first point ($\bar{n}_{e0} = 3.8 \times 10^{19}$ m^{-3}), whereas the high-density front is obvious at the third point ($\bar{n}_{e0} = 4.9 \times 10^{19}$ m^{-3}). Interestingly, at the second point ($\bar{n}_{e0} = 4.5 \times 10^{19}$ m^{-3}), the high-density front is not seen on POLARIS, but a luminous spot can already be observed with the CCD in the HFS SOL. This indicates that the high-density front initially forms in the SOL.

The evolution of the HFSHD front can be divided into two different phases with the continuous increase of density. The first phase is given the name 'growing phase'. At this phase, the high-density front is localized at the HFS edge while its magnitude grows. From CCD images 2–4 in figure 4(c), it is seen that the high-density front stays at the very edge of HFS during this phase. Meanwhile, its extent expands mainly along the poloidal direction. The process is confirmed by the variation of the C_{III} emission and electron density at the HFS edge in figures 4(a) and (b). Both the inward shift of the peak of the C_{III} emission from channel 1 (CH1) to channel 3 (CH3) and the time delay of the occurrence of the electron density nonlinear arising from -24 to -18 cm, are well explained by the growth and expansion of the high-density front. At the second phase, as the high-density front reaches a critical value ($\bar{n}_{e0} = 5.4 \times 10^{19}$ m^{-3}), the high-density front is found to quickly move poloidally, as can be seen in CCD images $5 \rightarrow 6$ in figure 4(c). The start-up of this poloidal movement can be identified by the roll-over of the electron density and C_{III} emission at the HFS edge, as shown in ⑤→⑥ of figures 4(a) and (b). The second phase is thus named as the 'moving phase'.

The above features comprise the typical characteristic of high-density front on J-TEXT. It is a common phenomenon in J-TEXT high density plasmas and the critical density threshold for the occurrence of the high-density front is well below that of the Greenwald DL. During the initial 'growing phase', the high-density front is quite stable at the HFS edge and will remain constant if the plasma density remains unchanged. The front can disappear if the plasma density backwards decreases down to the critical threshold. The poloidal movement of the high-density front during the subsequent 'moving phase' is quite rapid, which can be inferred by the step-like drop of the electron density at $r = -24$ cm. The macro-MHD instability and DL disruption usually occurs during the 'moving phase' of the high-density front. It seems that the movement of the high-density front deteriorates plasma confinement rapidly. By the way, the high-density front movement on J-TEXT is quite different to the MARFE movement observed on Frascati tokamak upgrade (FTU) L-mode and National Spherical Torus Experiment (NSTX) H-mode plasmas, which occurs at a density well below DL and is restorable [22, 23].

4. The role of plasma parameters on the formation of the high-density front

Figures 5(a) and (b) summarize the maximum achievable density from DL discharges on J-TEXT and the threshold density of high-density front formation in the discharges, with different plasma current (I_P) and the same toroidal magnetic field (B_T) on J-TEXT. For the maximum achievable density ($\bar{n}_{e0,DL}$), the experimental data from J-TEXT agrees well with the Greenwald scaling law [4], which means that the DL has a linear relationship with I_P (figure 5(a)). The DL at higher current is a little lower than would be expected from the linear relationship. This may be due to the enhanced magnetohydrodynamics (MHD) activity observed in $q_a < 4$ plasmas on the J-TEXT tokamak, which has been reported in [24].

The threshold density for the appearance of the high-density front ($\bar{n}_{e0,thres}$) is observed to have a similar linear dependence on I_P. Here, the time of appearance of the high-density front is measured as that when there is rise in the rate of change of increase of HFS edge electron density. For instance, in the plasma shown in figure 4, $\bar{n}_{e0,thres}$ is 4.6×10^{19} m^{-3}. The similar $\bar{n}_{e0,thres} \sim I_P$ and $\bar{n}_{e0,DL} \sim I_P$ relationships suggest that the high-density front might play an important role in setting the maximum achievable density on J-TEXT. In addition, as shown in figure 5(c), the local maximum density at the high-density front ($n_{e,HD}$), which is indicated by the line-average density at $r = -24$ cm, increases with I_P as well. That is consistent with the experimental observations on ASDEX Upgrade, where the density value of the high-density front increases with the heating power and plasma current [18, 25]. However, the relationship between $n_{e,HD}$ and I_P is not quite linear. The density of the high-density front tends to be saturated after I_P exceeds 150 kA.

Figure 6(a) presents the average edge electron density at the onset of the high-density front ($\bar{n}_{e_{edge,thres}}$) versus total plasma current. In order to exclude the influences of plasma displacement on density measurement, here, the edge electron density is taken as the mean value of line-average densities on the most LFS ($r = +24$ cm) and HFS ($r = -24$ cm) chords. The $\bar{n}_{e_{edge,thres}}$ increases with total plasma current, which is similar to the $\bar{n}_{e0,thres}$ (showed in figure 5(b)). But the difference is, the relationship of $\bar{n}_{e_{edge,thres}} \sim I_P$ is quite not as linear as $\bar{n}_{e0,thres} \sim I_P$. Obviously, the $\bar{n}_{e_{edge,thres}}$ increases faster at large I_P region (> 150 kA), than the low I_P area (< 150 kA). To divide the $\bar{n}_{e0,thres}$ by $\bar{n}_{e_{edge,thres}}$, we can obtain a rough peaking factor of density profile at the onset of the high-density front. As plotted in figure 6(b), the peaking factor of density distribution decreases largely in large I_P region. Combining with the relationship, it seems that a more peaked density profile is favorable to the formation of the high-density front. Behind the density distribution, the key parameter should be the radial transport. A peaked density profile means small perpendicular transport, and small edge temperature as well. And low enough temperature is one of demanded conditions for high-density front formation. This logic can qualitatively explain the nonlinear dependence of $\bar{n}_{e_{edge,thres}}$ on I_P.

All discharges showed in figures 5 and 6 are performed on the same day under similar experimental conditions. The plasmas are all fueled by continuous gas-puffing. The fueling rate remains constant in every single shot. The nose of the gas-puff is located at the bottom of plasma, meaning that the fueling source is in-out symmetrical. Therefore, to some extent, $\bar{n}_{e_{edge}}$ reflects the quantity of particles at the edge and $\bar{n}_{e0}$ represents the total amount of fueling. Figure 6(c) shows $\bar{n}_{e_{edge}}$ versus I_P, at the same central line-average density of $\bar{n}_{e0} = 2.5 \times 10^{19}$ m^{-3}, which is smaller than the threshold of the high-density front onset. The results indicate that there are more particles at edge in larger I_P plasmas, if the fueling amounts are the same. Moreover, the relationship of $\bar{n}_{e_{edge}}$ ($\bar{n}_{e0} = 2.5$) $\sim I_P$ is very similar to the observed relationship of $n_{e,HD} \sim I_P$ showed in figure 5(c). This implies that the amount of edge particles plays an important role in determining the density of the high-density front.
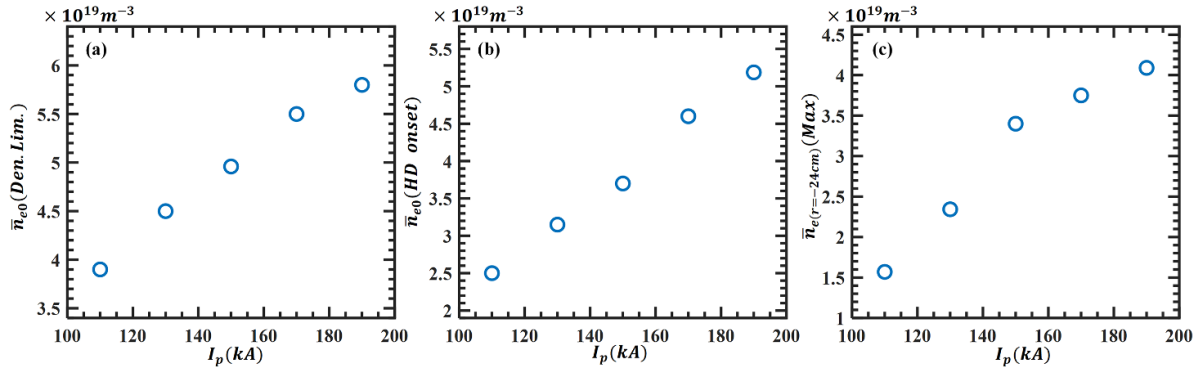
Figure 5. For a set of similar discharges with varying plasma current, the critical central line-average density at (a) the occurrence of the DL disruption; and (b) the high-density front plotted against the total plasma current. (c) The maximum density of the high-density front, represented by most inner edge line density, against the total plasma current for the same discharges.
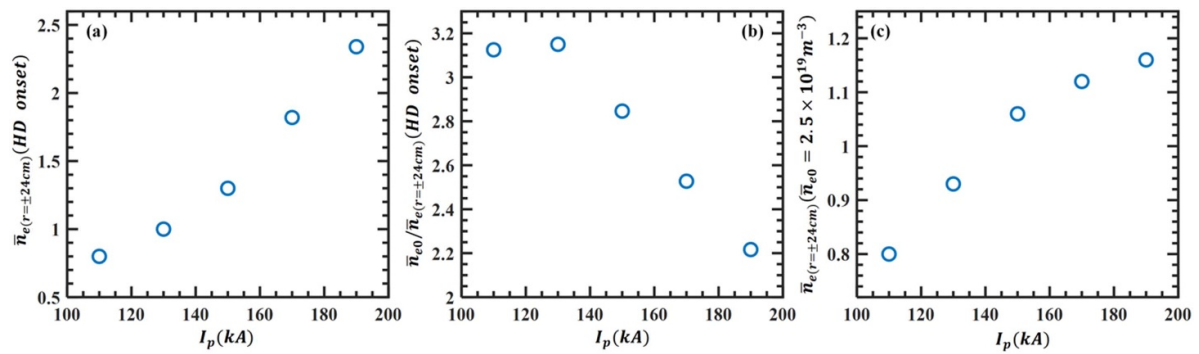
Figure 6. Corresponding to the same discharges in figure 5. The edge ($r = \pm 24$ cm) line-average electron density (a), and the ratio of central line-average density to the edge one (b), at the point of the onset of the high-density front. (c) The edge ($r = \pm 24$ cm) line-average electron density, at the point of central line-average density equals to $\bar{n}_{e0} = 2.5 \times 10^{19}$ m^{-3}.
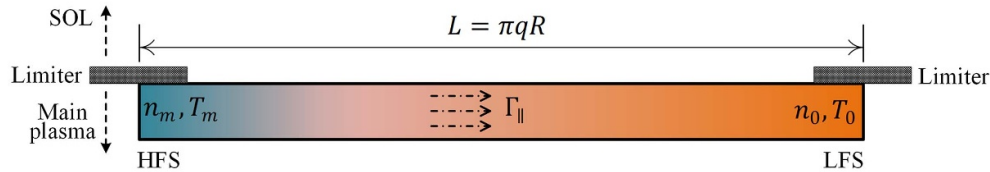

Figure 7. The one-dimensional flux tube model which connects the HFS and LFS edge.

Tokar *et al* [26] suggests that the Coulomb collisions in plasma ions is critical in the formation of cold-dense structure. In addition, we have known there exists a strong edge density asymmetry between the HFS and LFS after the high-density front appears, as presented by figures 2 and 3. The HFS-LFS density asymmetry indicates that a significant parallel density gradient forms at the edge. According to p 797 in [27] and p 194 in [28], the term of $L/\lambda_{ii} \propto n_e L/T_e^2$ can be utilized to represent the speed of particle diffusion from the HFS to LFS edge, furthermore to be related to the arise of high-density front. By straightening the magnetic field, the one-dimensional flux tube connecting the HFS and LFS edge, can be obtained as presented in figure 7. The connection length L can be estimated by simple form $L_{\text{HFS}-\text{LFS}} = \pi q_a R$, where q_a is the edge safety factor and R is the major radius. The HFS end, where

the high-density front locates, is assumed to has a higher density (n_m) than the LFS end (n_0).

In order to validate the effectiveness of the lumped term $n_e L/T_e^2$ in predicting the onset of high-density front, three shots with different I_P in figure 5 have been picked out. The traces of HFS-LFS density asymmetry, with $\bar{n}_{e0}$ and $n_e L/T_e^2$ are presented in figures 8(a)–(c) and (d)–(f) respectively. Here, $n_e = \bar{n}_e (\pm 24$ cm$)$ is measured by the POLARIS, and the T_e is relative temperature at $r = 23.5$ cm, measured by electron cyclotron emission. We have assumed the central temperature $T_{e0} = 800$ eV when $I_p = 150$ kA, $\bar{n}_{e0} = 2 \times 10^{19}$ m^{-3}. It is interesting that the high-density front appears at the similar value of $n_e L/T_e^2$, even though the three shots have quite different plasma current and density threshold. This experimental result suggests that the particle collision plays an important
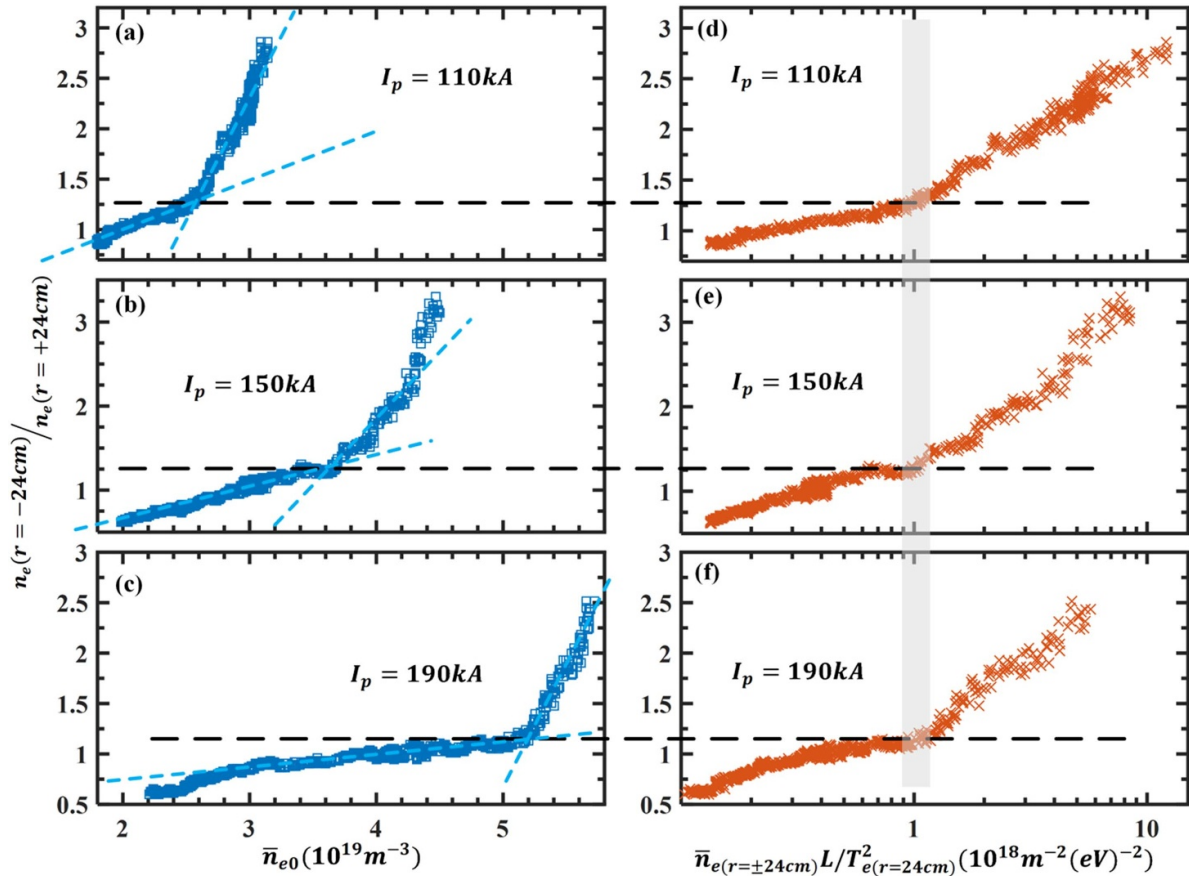
Figure 8. Traces of HFS-LFS density asymmetry against line-average density for (a) $I_P = 110$ kA; (b) $I_P = 150$ kA; and (c) $I_P = 190$ kA and against an edge collisionality parameter for (d) $I_P = 110$ kA; (e) $I_P = 150$ kA; and (f) $I_P = 190$ kA.

role in the formation of the high-density front. It should be noted that, the n_e and T_e used in calculation are parameters inside the LCFS, not the SOL region. That is because there are no measurements for SOL plasma on J-TEXT. And the appearance of high-density front is firstly detected by density measurement at $r = \pm 24$ cm. So, it is reasonable to use the local parameters where we observe it. Besides, the plasma horizontal position is almost symmetrical between the HFS and LFS limiter, and do not change shot by shot. And we have to point out that the formation of high-density front do not demand that the LCFS contact with the HFS limiter. Dedicated experiments have been performed on J-TEXT, to study the effects of plasma horizontal displacement on high-density front. When the plasma moves outwards and contact the LFS limiter, it is interestingly found that the high-density front still appears and even forms at a lower density threshold.

5. Discussion and summary

The high-density front has frequently been observed during high density pulses in the limiter J-TEXT tokamak when plasma density reaches a threshold. The high-density front forms at the SOL on the HFS and can have a local plasma density up to seven times larger than the separatrix density

in the LFS region. The appearance of the high-density front leads to highly poloidally asymmetric distributions of electron density and impurity radiation. As core density is continuously increased, the evolution of the high-density front on J-TEXT exhibits two different phases. In the first 'growing' phase, the high-density front stays localized at the HFS edge as it grows in magnitude and extent. The high-density front seems stable and does not impact plasma confinement, the local radiation level from bolometer measurement is low and almost neglectable comparing with core radiation. The characteristics of the high-density front at this stable phase are similar to the so-called HFSHD observed on divertor devices [15–17]. They are both formed at the HFS SOL region. The threshold density for the formation increases with plasma current. As all the discharges on J-TEXT are Ohmic heating only, the heating power depends broadly linearly on I_P. The results then are consistent with the observation on ASDEX Upgrade that the density of the high-density front increases with total heating power [18]. As density reaches a certain value, the high-density front is found to move quickly poloidally and evolves into an unstable 'moving' phase. The motion of the high-density front appears to deteriorate plasma confinement rapidly and is usually observed to be followed by plasma disruption. This suggests that the high-density front may play an important role in setting the maximum achievable density on J-TEXT.

The high-density front on J-TEXT appears to share some common characteristics with the well-known MARFE phenomenon, which has been widely detected on limiter and divertor devices. For instance, they both locate at the HFS edge, and have a locally high light-impurity emission and electron density. Also, they occur at high density plasmas, and are related to DL disruption. However, there are clear differences between them. Firstly, the MARFE is generally characterized by thermal instability, due to extremely high radiation power at the HFS edge. However, during the 'growing' phase, the high-density front on J-TEXT is thermally stable, and the loss of localized radiation remains at a very low level. In addition, the density threshold of MARFE onset is usually found to decrease if the plasma moves towards the HFS [13], and show weak relationship with toroidal magnetic field [29]. But the threshold of high-density front on J-TEXT increases while plasma displacement towards to HFS, and obviously decreases with the increase of toroidal field. Overall, the most important characteristic of the high-density front is the formation and growth of a local high-density region at the HFS edge, with the radiation not seeming to play an important role. Theoretical studies suggest that such cold-dense plasma structures can still form even when the radiation is completely removed and that the Coulomb collisions in plasma ions is critical in the formation of cold-dense structure [26]. A common critical collisionality for different discharges in J-TEXT seems in line with the theory. Although the high-density front shares some common features of reported MARFE phenomena, it appears that the high-density front is a particle accumulation behavior rather than a thermal instability. MARFEs may be the result of such structures forming in or moving into regions where the plasma temperature and impurity concentration are conducive for them to be radiatively unstable.

Studies of single null divertor configuration ASDEX Upgrade plasmas, including SOLPS simulations, show that the HFSHD front plays an important role in the fueling of the core plasma and thus is essential in understanding the SOL transport. The observation of the high-density front in a limiter device suggests that this may also be the case for limiter machines. Indeed, the high-density front seems more robust and has larger influence on plasma performance in J-TEXT. On J-TEXT, the plasma usually disrupts soon after the high-density front develops into the second 'moving' phase and the maximum achievable density is general well below the Greenwald density, $0.7n_G$. The formation and subsequent growth of the high-density front seems to set the machine operational limit. On ASDEX Upgrade, both simulation [17] and spectroscopic measurements [30] show that strong volumetric recombination starts to appear as the density increases, reducing the density in the inner divertor. The strong volumetric recombination provides a local plasma sink and stabilizes the growth of the high-density front. However, such a recombination sink is not expected to be significant in a limiter machine due to the lack a closure structure near the limiter target. Lack of a significant recombination sink could be the possible explanation of the more robust high-density front in HFS region.

In summary, the observation of the high-density front on J-TEXT sheds a new light on the understanding of SOL physics and provided a further challenge for modeling. Experimental and theoretical studies of the existence and phenomenology of the high-density front should not be limited to single null divertor devices. It also suggests that additional mechanisms should be considered to explain the formation and developing of the high-density front, apart from the self-amplifying process due to divertor structure and poloidal and perpendicular $E \times B$ drifts in the divertor.

Data availability statement

The data that support the findings of this study are available upon reasonable request from the authors.

ORCID iDs

Peng Shi ⬤ https://orcid.org/0000-0002-1853-0726
Hongjuan Sun ⬤ https://orcid.org/0000-0003-0880-0013
Zhifeng Cheng ⬤ https://orcid.org/0000-0001-6019-399X
Zhipeng Chen ⬤ https://orcid.org/0000-0002-8330-0070
Jingchun Li ⬤ https://orcid.org/0000-0001-9918-8880

References

[1] ITER Physics Expert Group on Divertor 1999 Chapter 4: power and particle control *Nucl. Fusion* **39** 2391–469
[2] Shimada M *et al* 2007 *Nucl. Fusion* **47** S1–17
[3] Wan Y *et al* 2017 *Nucl. Fusion* **57** 102009
[4] Greenwald M 2002 *Plasma Phys. Control. Fusion* **44** R27–53
[5] Lipschultz B, LaBombard B, Marmar E S, Pickrell M M, Terry J L, Watterson R and Wolfe S M 1984 *Nucl. Fusion* **24** 977–88
[6] Samm U 1999 *et al J. Nucl. Mater.* **266–9** 666–72
[7] Lipschultz B *et al* 1995 *J. Nucl. Mater.* **220–2** 50–61
[8] Xingya F 1990 *et al J. Nucl. Mater.* **176–7** 769–72
[9] Nishitani T, Ishida S, Hosogane N, Sugie T, Itami K and Takeuchi H 1990 *J. Nucl. Mater.* **176–7** 763–8
[10] Loarte A *et al* 1998 *Nucl. Fusion* **38** 331–71
[11] Gao X *et al* 2000 *J. Nucl. Mater.* **279** 330–4
[12] Lipschultz B 1987 *J. Nucl. Mater.* **145–7** 15–25
[13] de Vries P C, Rapp J, Schüller F C and Tokar' M Z 1998 *Phys. Rev. Lett.* **80** 3519–22
[14] Petrie T W *et al* 1997 *Nucl. Fusion* **37** 321–38
[15] Potzel S, Wischmeier M, Bernert M, Dux R, Müller H W and Scarabosio A 2014 *Nucl. Fusion* **54** 013001
[16] Manz P, Potzel S, Reimold F, Wischmeier M and Team A U 2017 *Nucl. Mater. Energy* **12** 1152–6

[17] Reimold F, Wischmeier M, Potzel S, Guimarais L, Reiter D, Bernert M, Dunne M and Lunt T 2017 *Nucl. Mater. Energy* **12** 193–9

[18] Potzel S *et al* 2015 *J. Nucl. Mater.* **463** 541–5

[19] Zhuang G *et al* 2011 *Nucl. Fusion* **51** 094020

[20] Zhuang G, Chen J, Li Q, Gao L, Wang Z J, Liu Y and Chen W 2013 *J. Instrum.* **8** C10019

[21] Zhang X L, Cheng Z F, Hou S Y, Zhuang G and Luo J 2014 *Rev. Sci. Instrum.* **85** 11E420

[22] Mazzotta C, Spizzo G, Pucella G, Giovannozzi E, Tudisco O, Apruzzese G, Bin W and Esposito B 2017 *Nucl. Mater. Energy* **12** 808–12

[23] Kelly F, Maingi R, Maqueda R, Menard J and Paul S 2009 *J. Nucl. Mater.* **390–1** 436–9

[24] Huang M, Hu Q, Shi P, Zhang X, Zhu L, Chen Z and Zhuang G 2016 *Plasma Phys. Control. Fusion* **58** 125002

[25] Potzel S *et al* 2015 *42nd EPS Conf. on Plasma Physics*

[26] Tokar M Z and Koltunov M 2012 *Phys. Rev.* E **85** 046412

[27] Wesson J 2011 *Tokamaks* (Oxford: Oxford University Press)

[28] Stangeby P C 2000 *The Plasma Boundary of Magnetic Fusion Devices* (Bristol; Philadelphia: Institute of Physics Pub)

[29] Pucella G *et al* 2013 *Nucl. Fusion* **53** 083002

[30] Reimold F *et al* 2015 *42nd EPS Conf. on Plasma Physics*